

Elastic wave propagation in an irregularly layered medium

Rossana Vai^a, José Manuel Castillo-Covarrubias, Francisco J. Sánchez-Sesma^{a,b,*},
Dimitri Komatitsch^c, Jean-Pierre Vilotte^c

^a*Instituto de Ingeniería, UNAM, Cd. Universitaria, Apdo 70-472, Coyoacán 04510, México D.F., Mexico*

^b*Centro de Investigación Sísmica, Carr. al Ajusco 203, col. H. de Padierna, Tlalpan 14200, México D.F., Mexico*

^c*Département de Sismologie (URA 195), Institut de Physique du Globe de Paris, 4, Place Jussieu, 75252 -Paris Cedex 05, France*

Received 11 June 1998; accepted 16 June 1998

Abstract

The indirect boundary element method (IBEM) is used to simulate wave propagation in two-dimensional irregularly layered elastic media for internal line sources. The method is based on the integral representation for scattered elastic waves using single layer boundary sources. Fulfillment of the boundary conditions leads to a system of integral equations. Results are obtained in the frequency domain and seismograms are computed through Fourier synthesis. In order to test and validate the method we present various comparisons between our results and the time series obtained analytically for a buried line source in a half-space and by using the recently developed spectral element method (SEM). © 1998 Elsevier Science Ltd. All rights reserved.

Keywords: Irregularly layered viscoelastic media; Synthetic seismograms; Diffracted–scattered wavefields

1. Introduction

The simulation of elastic wave propagation in the earth is of interest in many instances. For example, it can be crucial to correctly interpret field data aimed to identify deep buried structures, to locate underground resources and to interpret and forecast seismic ground motion amplifications due to local geology. The spatial variation of ground shaking has become evident after recent, well-documented earthquakes. Such is the case of the damage belt in Kobe during the Hyogo-ken Nambu event of January 1995 which was very likely produced by basin-induced surface waves (Kawase [1]).

Analytical solutions of elastic wave propagation problems are rare. The vectorial P - SV problem is generally solvable by numerical techniques only, while for few simple two-dimensional configurations the bulk of solutions of the scalar SH wave equation is applicable. These cases are quite unrealistic, yet they provide understanding of the physics of surface motion. To simulate wave propagation in more realistic circumstances, use must be made of numerical methods like finite differences, finite elements or spectral elements. The reader may find an account of these techniques in Sánchez-Sesma [2]. Here, let us just quote three among the latest publications: Ohminato and Chouet [5],

Moczo et al. [4] and Faccioli et al. [3], (for finite difference, finite difference combined with finite element and spectral element method, respectively). As far as laterally homogeneous layered media are concerned, the pioneering works of Haskell [6], Bouchon and Aki [7], Bouchon [8], Luco and Apsel [9] and Kennett [10] are essential references. Good specialized reviews are those of Chapman and Orcutt [11] and Muller [12]. Since then, a lot of work has been done modifying the existing methods to reduce computational time, speed up numerical convergence and gain numerical stability, mainly with the aim of efficiently solving inversion problems. However, realistic earth models imply irregularities of geometry, as well as of mechanical properties. For laterally irregular layered media a great variety of techniques has been used. In order to give, some perspective it is worth mentioning the following contributions. Aki and Larner [13] and Bouchon et al. [14] used the discrete-wave-number method and Boore [15] employed finite differences. Nolet et al. [16] used an approximated modal approach. Chen [17] proposed an extension of Kennett's method so that his formulation becomes particularly attractive as the number of layers increases. Pedersen et al. [18], Sánchez-Sesma et al. [20], Bouchon et al. [19] and Yokoi [21] calculated the seismic response using boundary integral equations. Druzhinin et al. [22] developed an approximate hybrid formulation with extremely reduced computational costs.

* Corresponding author. Tel: 00 52 5 6 223 460; Fax: 00 52 5 6 161 514.

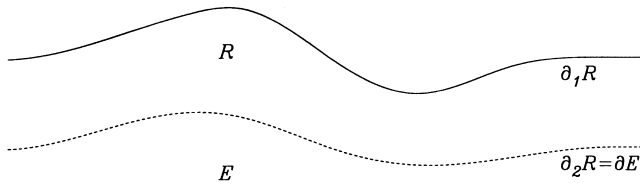


Fig. 1. Irregularly layered medium. An irregular homogeneous layer R rests on a homogeneous half-space E .

The goal of this paper is to explore the use of the Indirect Boundary Element Method (IBEM) when a buried line source excites a layered medium. The scattered fields are given in terms of boundary integrals. Introduction of boundary conditions and discretization of the integration paths lead to a system of linear equations. To properly account for the details of the wavefield, the discretization must be finer at larger frequencies, so that the size of the problem is approximately an increasing linear function of frequency. However, good results can be obtained with a relatively small computational effort. In what follows, the basic integral representation is given in detail and several examples are provided. Two of them are intended to test the method as the time series are compared with independent solutions; namely, the exact one obtained by Garvin [23] (for a buried line dilatational source in a half-space) and numerical results computed by Komatitsch and Vilotte [24] (an irregular layer over a half-space is solved using the spectral element method they have recently developed). Some new simulations for a sharp topographical profile and for an irregular layer are presented as well.

2. Integral representation

Consider the two-dimensional Euclidean space occupied by an elastic material and a continuous curve S , finite or infinite, in such a domain. Applying a harmonic force density $\phi_j(\xi)$ (where $j = 1$ or 3 and Cartesian coordinates are used) as excitation on S , the radiated elastic displacement can be written in terms of the integral.

$$u_i(\mathbf{x}) = \int_S \phi_j(\xi) G_{ij}(\mathbf{x}, \xi) dS_\xi \quad (1)$$

where $u_i(\mathbf{x})$ is the i th component of the radiated displacement at point \mathbf{x} ; $G_{ij}(\mathbf{x}, \xi)$ is the Green's function of the whole space, i.e. the displacement in the direction i at point \mathbf{x} due to the application of a unit harmonic force in the direction j at point ξ ; $\phi_j(\xi)$ is the force density in the direction j ; here and hereafter the usual sum convention for repeated indices is used. Therefore, $\phi_j(\xi) dS_\xi$ is clearly a force distribution at the surface S . Suffixes in the differential operator denote the spatial variable over which the integral is performed. This integral representation can be obtained from Somigliana's identity (Sánchez-Sesma and Campillo [25]). Kupradze [26] proved that the displacement field is continuous across S if $\phi_j(\xi)$ is continuous along S .

By application of Hooke's law and Cauchy's equation we have

$$t_i(\mathbf{x}) = c \phi_i(\mathbf{x}) + \int_S \phi_j(\xi) T_{ij}(\mathbf{x}, \xi) dS_\xi \quad (2)$$

where $t_i(\mathbf{x})$ is the i th component of traction associated to a direction $\mathbf{n}(\mathbf{x})$; $c = 0.5$ if \mathbf{x} tends to the smooth boundary S from inside, that is to say to the surface with outward directed unit normal $\mathbf{n}(\mathbf{x})$ ($c = -0.5$ if the normal has opposite direction), $c = 0$ if \mathbf{x} is not at S ; $T_{ij}(\mathbf{x}, \xi)$ = traction Green's function, i.e. the traction in the direction i at a point \mathbf{x} with associated direction $\mathbf{n}(\mathbf{x})$ and due to the application of a unit force in the direction j at ξ on S .

Green's functions for displacement and traction of two-dimensional problem are expressed by means of cylindrical Hankel's functions. Recalling Sánchez-Sesma and Campillo [25], we write

$$G_{ij} = A \delta_{ij} - B(2\gamma_i \gamma_j - \delta_{ij})$$

$$T_{ij} = \frac{\mu}{r} \left\{ \left[-4B + \lambda \frac{D(\omega r/\alpha)}{2\mu\alpha^2} \right] \gamma_j n_i + \left[-4B + \frac{D(\omega r/\beta)}{2\beta^2} \right] \times [\gamma_i n_j + \gamma_k n_k \delta_{ij}] \right\} + \frac{\mu}{r} \{ (C + 16B) \gamma_i \gamma_j \gamma_k n_k \}$$

where

$$A = \frac{1}{i8\rho} \left[\frac{H_0^{(2)}(\omega r/\alpha)}{\alpha^2} + \frac{H_0^{(2)}(\omega r/\beta)}{\beta^2} \right]$$

$$B = \frac{1}{i8\rho} \left[\frac{H_0^{(2)}(\omega r/\alpha)}{\alpha^2} - \frac{H_0^{(2)}(\omega r/\beta)}{\beta^2} \right]$$

$$C = \frac{D(\omega r/\alpha)}{\alpha^2} - \frac{D(\omega r/\beta)}{\beta^2}$$

$$D(p) = \frac{i}{2\rho} p H_1^{(2)}(p)$$

λ and μ are the Lamé's constants; ρ is the mass density; α and β are P and S wave velocity, respectively; $r = \sqrt{(x_1 - \xi_1)^2 + (x_3 - \xi_3)^2}$; $\gamma_j = (x_j - \xi_j)/r$; δ_{ij} is the Kronecker's delta and $H_m^{(2)}(\cdot)$ is the Hankel's function of the second kind and order m .

Green's functions have a deep physical meaning as they give essential, complete information from which we can compute any dynamic field if appropriate boundary conditions are imposed. When frequency tends to zero the dynamic field, expressed by means of Green's functions, tends to its static counterpart (see e.g. Love [27]).

3. Formulation of the problem

Consider now an elastic half-space E with an elastic layer R (Fig. 1). The free surface of the layer is denoted by $\partial_1 R$,

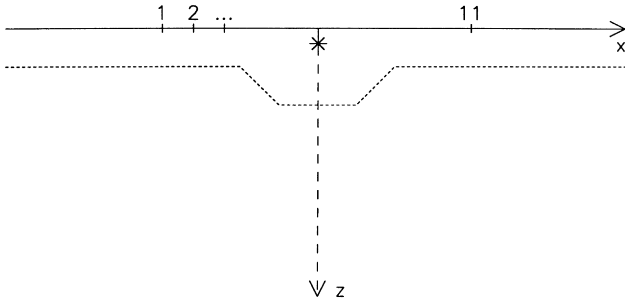


Fig. 2. Transparent layer model used to compare the Garvin's solution [23] and our results. Regions R and E have the same properties. The interface between the two media has the trapezoidal shape defined in the text. The source is located just under the free surface so that Rayleigh waves clearly emerge.

the interface between the two media is named $\partial E = \partial_2 R$. Because of linearity, the total ground motion can be expressed by the superposition of a known *reference* solution with unknown diffracted-scattered wavefields

$$u_i = u_i^{(0)} + u_i^{(d)} \quad (3)$$

where $u_i^{(0)}$ is the reference solution (i.e. the solution for the source in the absence of irregularities) and $u_i^{(d)}$ is the diffracted-scattered displacement fields.

When a line source excites the model, $u_i^{(0)}$ is zero everywhere except in the medium where the source is located. In this medium the reference solution is the radiated field generated by the source. Diffracted-scattered fields, which satisfy Sommerfeld's radiation condition, can be computed using the integral form of Eq. (1), if the force densities are known.

Superposition of effects can also be used to represent tractions

$$t_i = t_i^{(0)} + t_i^{(d)} \quad (4)$$

where $t_i^{(0)}$ corresponds to the reference solution, whereas $t_i^{(d)}$ to the diffracted-scattered fields.

Tractions and displacements have to be continuous at the interface between media and tractions must be null at the free surface. These three conditions, respectively, allow us to write a system of integral equations for the unknown force densities:

$$\begin{aligned} \frac{1}{2} \phi_i^E + \int_{\partial E} \phi_j^E T_{ij}^E dS_\xi + \frac{1}{2} \phi_i^R - \int_{\partial R} \phi_j^R T_{ij}^R dS_\xi \\ = -t_i^{(0)E} + t_i^{(0)R}, \quad \mathbf{x} \in \partial_2 R \end{aligned} \quad (5)$$

$$\int_{\partial E} \phi_j^E G_{ij}^E dS_\xi - \int_{\partial R} \phi_j^R G_{ij}^R dS_\xi = -u_i^{(0)E} + u_i^{(0)R}, \quad \mathbf{x} \in \partial_2 R \quad (6)$$

$$-\frac{1}{2} \phi_i^R + \int_{\partial R} \phi_j^R T_{ij}^R dS_\xi = t_i^{(0)R}, \quad \mathbf{x} \in \partial_1 R \quad (7)$$

where the superscript denotes the medium for which the associated quantity is defined and $\partial R = \partial_1 R + \partial_2 R$.

In general, for multilayered media, the system to be solved is composed of $2N + 1$ equations, where N is the number of layers. Continuity of displacements and tractions at each interface has to be enforced; the new equations would have the structure of Eqs. (5) and (6).

From a mathematical point of view, the system of Eqs. (5)–(7) allows us to find out the force density distributions which, substituted back into Eq. (1), give the diffracted displacement field. Numerically, these integral equations still present some difficulties because of their continuous integrand functions, because of the singularity of the Green functions and because of the infinite integration paths. To solve these problems the following procedure can be adopted. Each curved surface is discretized into linear segments which size depends on the shortest wavelength taken between those of the two joining media. Along the segments, the force density variation is prescribed and Gaussian integration (or analytical integration, where the Green function is singular) is performed. More details about the discretization procedure can be found in Sánchez-Sesma et al. [28] and in Sánchez-Sesma and Campillo [25]. The results we present are obtained choosing the segment size minor than one sixth of the wavelength, ϕ is assumed constant on each segment and three Gaussian points are used. With such parameters, accurate solutions can be obtained. As far as the infinite integration paths are concerned we have no choice: surfaces have to be finite. The IBEM can be seen as the numerical realization of the Huygen's principle. Thus, to reconstruct, say, a given wave front, all the points of the infinite discontinuity surface act as sources and radiate energy. If surfaces are truncated, the solution lacks the lateral contributions and the edges play as diffractor points which generate spurious waves. The artificial perturbations are characterized by small amplitudes and their reflections inside the model are negligible. Errors are mainly associated to back-scattering waves generated at the boundary edges. Different constructs can be adopted to eliminate, or much reduce, this noise. The simplest solution is to choose a surface length large enough so that the fictitious waves fall outside the observational space-time window. Alternatively, one can play with the quality factor increasing damping near the edges [29], or approximate the integral on the infinite surface using an analytical asymptotic device [30]. The results we present are obtained without using any artifice. Since the computational effort increase with surfaces length, we just look for a trade-off between economy and precision.

By means of the described procedure the infinite number of radiating sources is reduced to a finite number of unknowns and the set of integral equations becomes a linear system of equations.

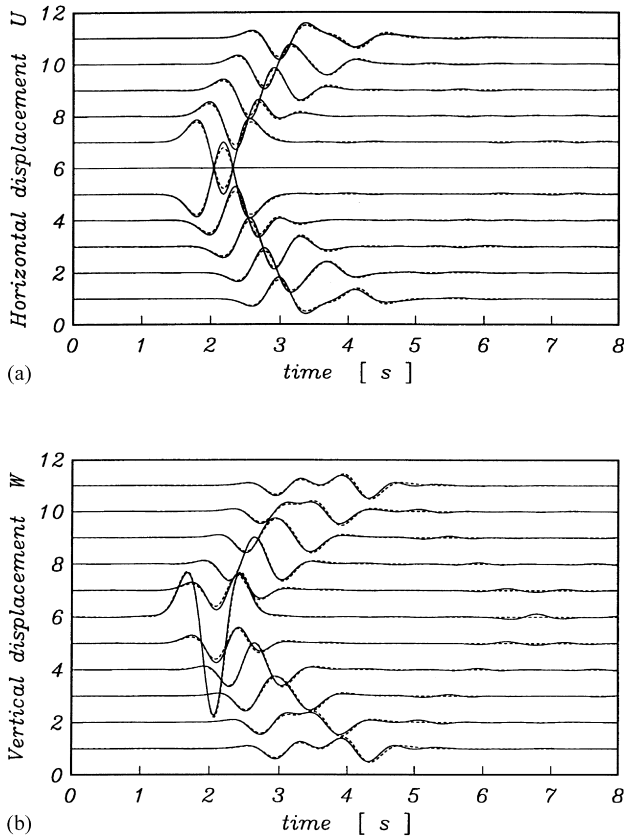


Fig. 3. Comparison between our results (continuous line) and Garvin's solution (dashed line). The computations were performed for the model of Fig. 2. The agreement between the traces is very good.

4. Testing of the method

For a dilatational line source of impulsive type buried in a homogeneous half-space, Garvin [23] expressed surface time displacements by exact closed algebraic formulas. To validate our method we use this analytical solution, convolved with a source time function. Therefore, with the IBEM code, we calculate synthetic seismograms and compare them with Garvin's time traces. In the example

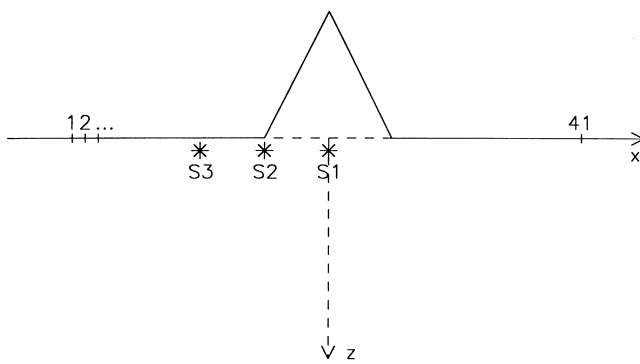


Fig. 4. A triangular hill is used to assess the effects of an irregular topography. Computations are made for each one of the three depicted sources independently.

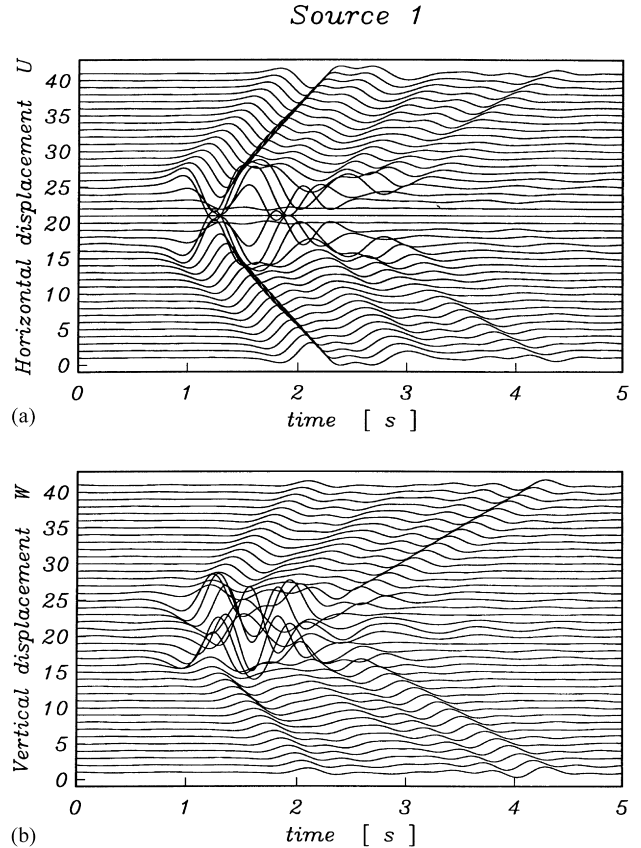


Fig. 5. Horizontal and vertical displacements computed at the free surface for the model of Fig. 4 excited by the deep source 1. The symmetry of geometry is reflected in the symmetry of the vertical traces and in the antisymmetry of the horizontal traces.

we present here, we solve an irregular layer with the same properties of the half-space, so that consistency of our scheme is also tested, and a flat free surface (Fig. 2). The irregularity has a trapezoidal shape: its major base measures 2 km and the minor one 1 km; the depth of the layer varies from 0.5 to 1 km; the discretized surface covers 3 km on each side of the symmetry axis. Wave velocities are of 1 and 2 km s⁻¹ for S and P waves, respectively. No attenuation is considered. The source is located on the symmetry axis at a depth of 0.2 km. We use an array of 11 equally spaced receivers with an offset of 0.4 km. The excitation is provided by a Ricker pulse, which is analytically expressed by $r(t) = (a^2 - 1/2) \exp(-a^2)$ and $a = \pi(t - t_s)/t_p$; we choose $t_p = 1$ s as characteristic period and $t_s = 2$ s. The comparison between Garvin's and IBEM solutions shows a very good agreement (Fig. 3). We can identify spurious Rayleigh waves arrivals, which represent an edge effect due to the finite length of the discretized surface. Free surface edges are the only source of appreciable artificial diffraction. Both low and high frequencies are equally affected by noise. Varying the total length of the discretized surfaces, transfer functions maintain the same pattern but amplification levels reveal little differences. The solution converges increasing the relation between discretized and

Source 2

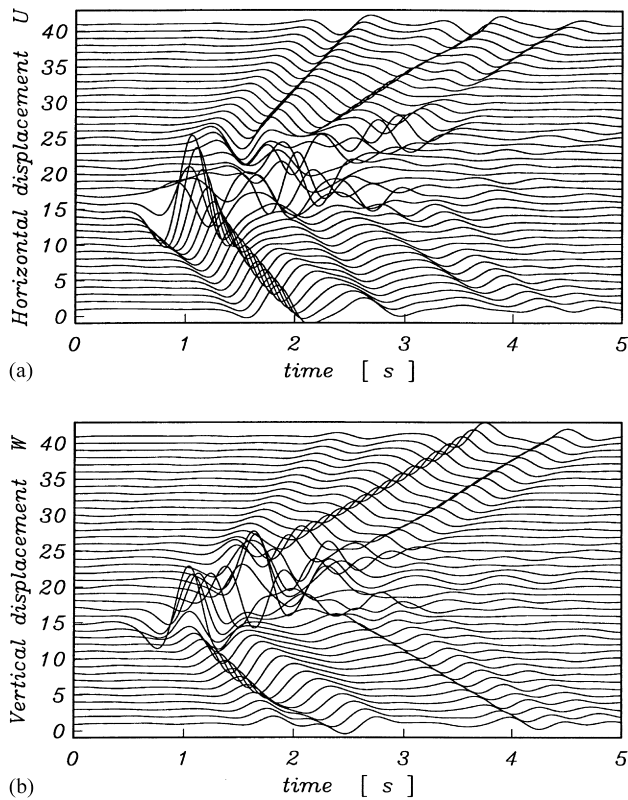


Fig. 6. Horizontal and vertical displacements computed at the free surface for the model of Fig. 4 excited by source 2. The source is just under the base edge of the hill. Part of the energy radiates inside the relief and part immediately reaches the free surface.

observation region. At the free surface, the peak amplitude of these fictitious displacements is of about one tenth of the maximum value of direct Rayleigh waves. For buried receivers the difference is still greater.

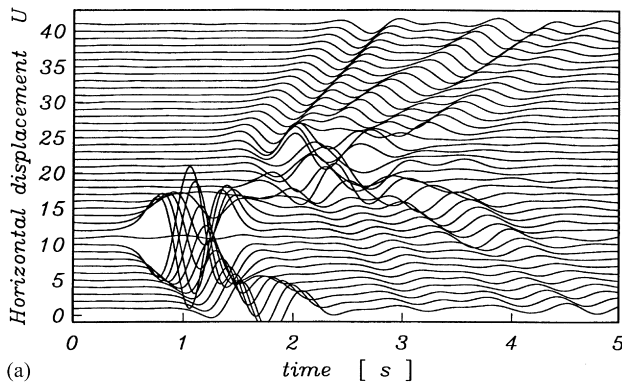
5. Examples

To assess topographic effects we study an homogeneous half-space with irregular surface. In this model we are not introducing any transparent layer; thus, the free surface is the only boundary condition we consider. In fact, the formulation we presented is an extension of that used to solve irregular topography problems. Since no interface is defined, only Eq. (7), the free surface condition, is required; all the superscripts are turned to E and the integration path is ∂E . We analyze a triangular mountain 2 km high and 2 km wide at the base, the limits of the discretized boundary are placed at 6 km at each side from the symmetry axis (Fig. 4). Three different sources are considered: the first one on the symmetry axis, the other two at 1 and 2 km away from it, all of them are located at a depth of 0.2 km under the flat surface level. S wave velocity is 2 km s^{-1} and ν is $1/4$. Quality factor for both P and S waves is 10 000, i.e. no

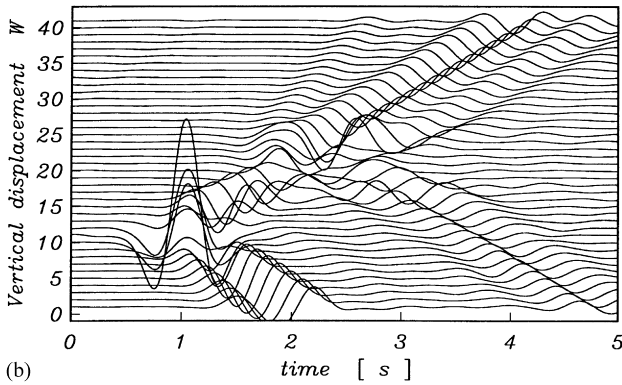
attenuation is considered. Forty-one equally spaced receivers are placed symmetrically, covering a distance of 8 km, the first station is at 2 km from the surface edge. To compute synthetics, we use a Ricker pulse characterized by $t_p = 0.75 \text{ s}$ and $t_s = 1 \text{ s}$, results are shown in Figs. 5–7. Although source depth is the same for the three examples we analyze, vertical displacement amplitude is very different. Indeed, for major vertical distance between free surface and source minor amplifications are estimated (example 1 against 2 and 3), for major energy concentration larger amplifications are obtained (in the second case energy partially radiate inside the mountain, whereas in the third example direct upgoing waves are reflected from the flat free surface). As far as horizontal displacement is concerned, we can observe A clear symmetry when the source is located on the geometrical symmetry axis (first case) or below a locally symmetric surface (third case). In this last example symmetry is broken as soon as back propagating waves, diffracted by the mountain, arrive at the stations. No matter which case we consider, the synthetic pattern is remarkably different for mountain and flat surface receivers. On the flat surface we can identify the direct P wave arrival, the Rayleigh waves contribution to this arrival is neatly separated far away from the source. Then we can appreciate two main Rayleigh waves groups, both associated with an elliptical retrograde particle displacement.

In order to study wave propagation in a laterally irregular layered medium we compare the results obtained with the IBEM and with the SEM. The spectral element method will be presented elsewhere (see Komatitsch et al. [31]). Some results obtained for the models of Figs. 8 and 10 are shown in Figs. 9 and 11; in both cases agreement is excellent. We assume S wave velocity (β) equal to 0.5 km s^{-1} in the layer and to 1.5 km s^{-1} in the half space; in both cases α , the P wave velocity, is twice β . No damping is introduced. We examined sources located inside the layer as in the half-space, but the simulations presented here correspond just to the sources S1[$-1 \text{ km}, 3 \text{ km}$] and S2[$-1 \text{ km}, 1.5 \text{ km}$]. Fifty-one equally spaced stations cover 2 km on the free surface in both directions from the symmetry axis. Ricker pulse central frequency is 0.75 Hz ($t_p = 1.3333 \text{ s}$) and $t_s = 1.4 \text{ s}$. We first analyze the effect produced by an irregular interface described by the function $z = 1 + 0.5[\sin(\pi(x + 1)/2)]^2$, for $-1 \text{ km} < x < 1 \text{ km}$; the discretized free surface is truncated at $x = \pm 6 \text{ km}$ (Fig. 8). The number of unknowns we use varies from 77 to 890 (for the minimum and maximum frequency, respectively), while the spectral method requires a grid made of 22176 points. The solution we present is obtained computing just 128 frequencies, while the spectral method is run through 4000 time steps. More details on the model used in the SEM simulation can be found in Komatitsch et al. [31]. The two methods give the displacement field in the whole domain, but the number of unknowns they manage differs in orders of magnitude. In Fig. 9 we present the results obtained for source 1. We can observe significant amplification effects

Source 3



(a)



(b)

Fig. 7. Horizontal and vertical displacements computed at the free surface for the model of Fig. 4 excited by the superficial source 3. Motion amplification is bigger than in the two previous cases (Figs. 5–7 are all plotted at the same scale).

at the center of the valley. This phenomenon is remarkable both in vertical and horizontal motion. First arrival at the center of the valley has a vertical amplitude of two times the one computed for edge receivers; horizontal displacement at different receivers shows smaller variation. If the layer were flat, the same source would not produce significant surface waves, we would see five *P* arrivals (the direct wave and its *P* reflections as it bounces up and down the layer), no significant *SV* conversion would be appreciable and superficial Rayleigh waves would appear only after 10 s. Vertical

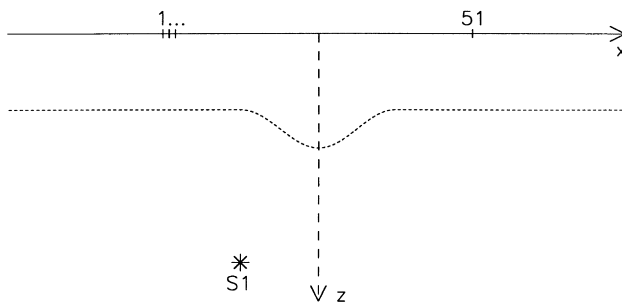
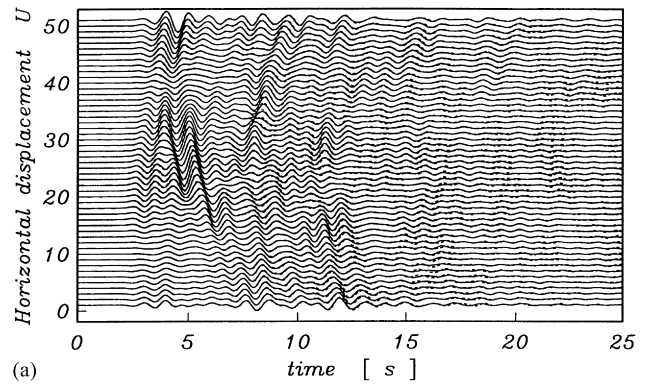
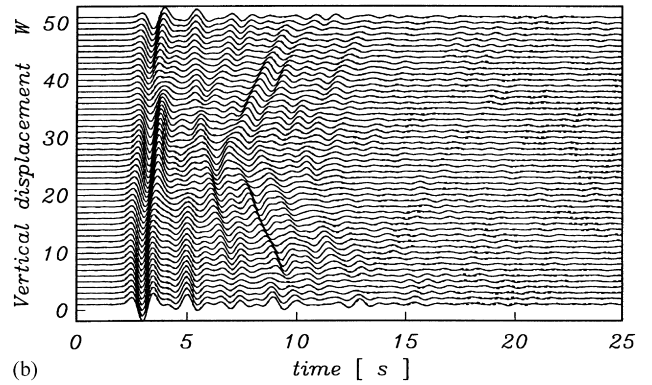


Fig. 8. Layer characterized by flat free surface, irregular smooth interface and mechanical properties different from half space. The model was used to validate our technique with another numerical method (the SEM).

Source 1



(a)



(b)

Fig. 9. Synthetic seismograms at the free surface for the model of Fig. 8. Our results (continuous line) and the solution obtained by the spectral element method (dashed line) are compared. The agreement between the traces is impressive.

motion would prevail on the horizontal and the shadowed zone on the right edge of the basin wouldn't appear. The smooth irregularity of the interface is responsible for important rising of superficial waves.

The second model we use to compare SEM and IBEM results is obtained from the former introducing an irregular free surface $z = -0.5[\sin(\pi(x + 1)/2)]^2$ for $-1 \text{ km} < x < 1 \text{ km}$, Fig. 10. In this case, to reduce computational costs, surfaces were truncated at $x = \pm 4 \text{ km}$. For the characteristics of the model used in the SEM simulation reference is

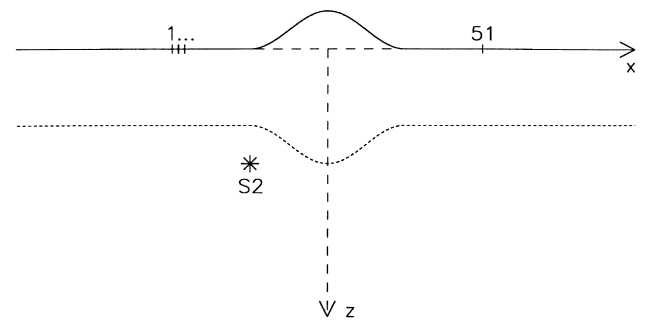


Fig. 10. Layer characterized by irregular free surface and interface, layer mechanical properties are different from half space properties.

Source 2

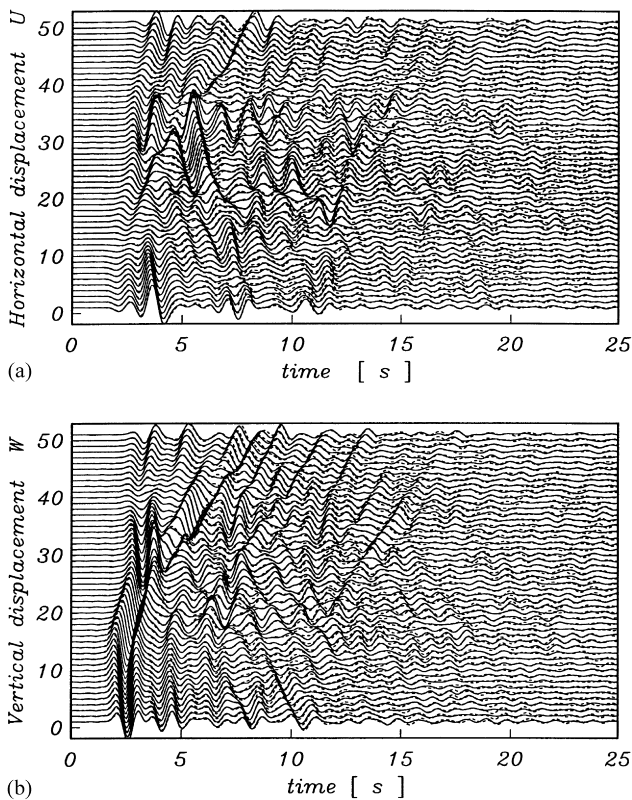


Fig. 11. Synthetic seismograms at the free surface for the model of Fig. 10. Our results (continuous line) and the solution obtained by the spectral element method (dashed line) are compared. Edge effects introduce noise in the IBEM results, therefore, late phases and amplitudes are not so precisely reproduced as those during the first few seconds of motion.

made to Komatitsch et al. [31]. The synthetics we present (Fig. 11) are obtained for source 2. Agreement between the two solutions is not as good as in the former example. The differences between the two calculations are due to edge effects. Two effects contribute to the discrepancies in late phases and amplitudes. There is interference between waves diffracted at the edges and inside the valley. For the example we presented in Fig. 1, it was possible to recognize backward propagating waves, produced by edge effects; now identification of different groups is no longer possible. Moreover, we have already explained that truncating the surfaces we neglect the contribution of radiating sources, if the discretized surface is too short a considerable amount of waves is lost and synthetics cannot be precise. The perturbations travel time governs the time window in which the solution is good. The motion predicted for the first seconds, when displacement reaches its maximum amplitude, is very well reproduced. Considering the first 5 s, motion computed at lateral receivers is quite similar to the one calculated with the model of Fig. 8; displacement field is dominated by direct arrival and major reflections at the interface. Later on, diffracted-scattered fields generated at the irregular topography interfere modifying motion pattern. Comparing

with the previous example, inside the valley we notice an increased amplification level and longer duration, the double irregularity is such that diffracted and scattered waves cannot be easily radiated to infinity.

6. Conclusions

We have presented an IBEM application to layered media excited by a dilatational line source. Excellent results were obtained with minimum computational effort. In further applications to inversion problems, the efficiency of the method should be increased optimizing the system solution in order to reduce memory requirements and, more importantly, computational times. The examples we presented evince significant effects due to surface geology. Their correct assessment is crucial in the analysis of seismic risk.

Acknowledgements

Thanks are given to K. M. Rasmussen and to A. C. Carrasco for the critical reading of the manuscript and for their keen suggestions. This research was partially supported by Dirección General de Asuntos de Personal Académico of UNAM, Mexico, (under Grant IN-108295) and by Fondazione Confalonieri, Italy.

References

- [1] Kawase H. Site effects observed during the Hyogo-ken Nanbu earthquake of 1995 and strong motion simulation including the basin-edge effect. in: Proceedings of the 11th World Conference on Earthquake Engineering, Acapulco, Mexico, June 1996. Oxford: Pergamon Press, 1996:1328.
- [2] Sánchez-Sesma FJ. Strong motion and site effects. In: Beskos DE, Anagnostopoulos SA, editors. Computer analysis and design of earthquake resistant structures. A handbook. Southampton: Computational Mechanics Publications, 1996.
- [3] Faccioli E, Maggio F, Paolucci R, Quarteroni A. 2D and 3D elastic wave propagation by a pseudo-spectral domain decomposition method. *J Seis* 1997;1:237–251.
- [4] Moczo P, Bystrický E, Kristek J, Carcione JM, Bouchon M. Hybrid modeling of *P*-*SV* seismic motion at inhomogeneous viscoelastic topographic structures. *Bull Seis Soc Am* 1997;87:1305–1323.
- [5] Ohminato T, Chouet BA. A free-surface boundary condition for including 3D topography in the finite difference method. *Bull Seis Soc Am* 1997;87:494–515.
- [6] Haskell NA. The dispersion of surface waves on multilayered media. *Bull Seis Soc Am* 1953;43:17–34.
- [7] Bouchon M, Aki K. Discrete wave-number representation of seismic-source wave fields. *Bull Seis Soc Am* 1977;67:259–277.
- [8] Bouchon M. A simple method to calculate Green's functions for elastic layered media. *Bull Seis Soc Am* 1981;71:959–971.
- [9] Luco JE, Apsel RJ. On the Green's functions for a layered half-space, part 1. *Bull Seis Soc Am* 1983;73:909–929.
- [10] Kennett BLN. Seismic wave propagation in stratified media. Cambridge: Cambridge University Press, 1983.
- [11] Chapman CH, Orcutt JA. The computation of body wave synthetic seismograms in laterally homogeneous media. *Rev Geophys* 1985;23(2):105–163.

- [12] Müller G. The reflectivity method: a tutorial. *Geophys J Int* 1985;58:153–174.
- [13] Aki K, Larner KL. Surface motion of a layered medium having an irregular interface, due to incident plane *SH* waves. *J Geophys Res* 1970;75:933–954.
- [14] Bouchon M, Campillo M, Gaffet S. A boundary integral equation-discrete wavenumber representation method to study wave propagation in multilayered media having irregular interfaces. *Geophysics* 1989;54:1134–1140.
- [15] Boore DM. Finite difference methods for seismic wave propagation in heterogeneous materials. In: *Methods in computational physics*. New York: Academic Press, 1972;11:1–37.
- [16] Nolet G, Sleeman R, Nijhof V, Kennett BLN. Synthetic reflection seismograms in three dimensions by a locked mode approximation. *Geophysics* 1989;54:350–358.
- [17] Chen X. Seismograms synthesis for multilayered media with irregular interfaces by global generalized reflection/transmission matrices method — I. Theory of 2-D *SH* case. *Bull Seis Soc Am* 1990;80:1696–1724.
- [18] Pedersen HA, Sánchez-Sesma FJ, Campillo M. Three-dimensional scattering by two-dimensional topographies. *Bull Seis Soc Am* 1994;84:1169–1183.
- [19] Bouchon M, Schultz CA, Töksoz MN. A fast implementation of boundary integral equation methods to calculate the propagation of seismic waves in laterally varying layered media. *Bull Seis Soc Am* 1995;85:1679–1687.
- [20] Sánchez-Sesma FJ, Vai R, Castillo-Covarrubias J, Luzon F. Respuesta sísmica de medios estratificados irregulares usando el método indirecto de elementos de frontera: Aplicación al estudio de la influencia de la estructura profunda en la respuesta sísmica de la cuenca de México. In: Medina-Martínez F, Delgado-Argole LA, Suarez-Reinoso G, editors. *La sismología en México: 10 años después del temblor de Michoacán del 19 de Septiembre de 1985 ($M = 8.1$)*, Monografía no. 2 de la Unión Geofísica Mexicana, September 1995. Unión Geofísica Mexicana.
- [21] Yokoi T. An indirect boundary element method based on recursive matrix operation to compute waves in irregularly stratified media with infinitely extended interfaces. *J Phys Earth* 1996;44:39–60.
- [22] Druzhinin A, Pedersen H, Campillo M, Kim W. Elastic Kirchhoff–Helmholtz synthetic seismograms. *Pure Appl Geophys* 1998;151:17–45.
- [23] Garvin WW. Exact transient solution of the buried line source problem. *Proc R Soc, London Ser A* 1956;234:528–541.
- [24] Komatitsch D, Vilotte JP. The spectral element method: an efficient tool to simulate the seismic response of 2-D and 3-D geological structures. *Bull Seis Soc Am* 1998;88:368–392.
- [25] Sánchez-Sesma FJ, Campillo M. Diffraction of *P*, *SV* and Rayleigh waves by topographic features: a boundary integral formulation. *Bull Seis Soc Am* 1991;81:2234–2253.
- [26] Kupradze VD. Dynamical problems in elasticity. In: Sneddon IN, Hill R, editors. *Progress in solid mechanics*. Amsterdam: North-Holland, 1963:3.
- [27] Love AEH. *A treatise on the mathematical theory of elasticity*, 4th edn. New York: Dover Publications, 1944.
- [28] Sánchez-Sesma FJ, Ramos-Martínez J, Campillo M. An indirect boundary element method applied to simulate the seismic response of alluvial valleys for incident *P*, *SV* and Rayleigh waves. *Earthquake Engng Struct Dyn* 1993;22:279–295.
- [29] Pedersen HA. Étude de la diffraction tridimensionnelle des ondes sismiques dans des structures à géométrie bidimensionnelle, développement théorique et applications. Ph.D. thesis, Université Joseph Fourier, Grenoble, 1994.
- [30] Yokoi T, Takenaka H. Treatment of an infinitely extended free surface for indirect formulation of the boundary element method. *J Phys Earth* 1995;43:79–103.
- [31] Komatitsch D, Vilotte JP, Vai R, Castillo-Covarrubias JM, Sánchez-Sesma FJ. The Spectral Element method for elastic wave equations: application to 2D and 3D seismic problems. *Int J Numer Meth Engng* (submitted).